Proceedings of the Sixteenth International Conference on
Computational Structures Technology
Edited by: P. Iványi, J. Kruis and B.H.V. Topping
Civil-Comp Conferences, Volume 14, Paper 2.2
Civil-Comp Press, Edinburgh, United Kingdom, 2026
ISSN: 2753-3239, doi: 10.4203/ccc.14.2.2

FE Numerical Errors in Lattice Metastructure Dynamics: Insights from Two Distinct Cases

I. Martínez-Terés[1,2], K. V. Bhat[2], P. Pflueger Tejero[1,2], J. Garcia-Martinez[1,2] and F. J. Montáns[2]

[1] Structures and Mechanisms Area, Instituto Nacional de Técnica Aeroespacial, Torrejon de Ardoz (Madrid), Spain
[2] Escuela Técnica Superior de Ingeniería Aeronáutica y del Espacio, Universidad Politécnica de Madrid, Spain

Abstract

The influence of numerical errors associated with finite element modelling on the dynamic response of lattice-based mechanical metamaterials (MMM) is studied in this work. Dispersion diagrams for mechanical characterization were introduced some decades ago, but it is only in recent years that they constitute an established approach for the characterization of the dynamic mechanical behaviour of lattice-based structures.

The recent development of MMM is accelerated by advances in additive manufacturing. However, the manufacturing process inevitably introduces dimensional deviations between the nominal design geometry and the as-built structure. Such geometric discrepancies can be interpreted, from a modelling perspective, as perturbations in nodal positions within the finite element discretization. Therefore, the present study is directly concerned with quantifying how these geometry-induced numerical deviations affect the resulting dispersion diagrams depending on the location of the error.

In this context, the effect of small deviations of the spatial positioning of the nodes in the dispersion diagrams is analysed. The influence of two distinct cases that lead

to significantly different outcomes is presented in this work: nodes subjected to Floquet–Bloch boundary conditions, and nodes located within the interior of the lattice that are not affected by the imposed boundary conditions

Keywords: Additive manufacturing, metamaterial, dispersion diagrams, band gaps, dynamic response, finite element analysis

1 Introduction

Dispersion diagrams (DD) [1,2] are a common tool to dynamically characterize lattice-based mechanical metastructures (MMM) [3,4]. After imposing Floquet-Bloch boundary conditions at the boundaries of a single cell, the behaviour of an infinite array of cells can be simulated using limited computation resources. This differs from real structures, which are finite, but under the hypothesis of a sufficient high number of cells (which can be stablished in one, two, or the three directions), the DD adequately identifies bandgaps where the current structure will present an attenuation of the vibration transmitted in that frequency band.

The boundary conditions must be applied in matching nodes, i.e. the link is stablished between two nodes that must be exactly in the same position along the infinite array. For example, in finite elements models, if a node exists in the centre of a cubic lattice face, another one must exist in the centre of the opposite face, so that they can be adequately linked. This requirement imposes either a limitation on the cell geometry – with symmetry in 1,2 or three directions – or a checking and modification of the boundary nodes position after meshing. The latter case may not be easily available in 3D geometries, and in practice, it depends on the available meshing tool.

Additionally, the usual intricate geometries of lattice-based MMM can only be manufactured through additive manufacturing. The dimensional accuracy of such final products still does not reach the standards of regular manufacturing methods, entailing significant deviations from the nominal geometry. These deviations come from diverse sources related to the specific additive manufacturing process: porosity, surface roughness, waviness, section reduction, broken struts, non-melted particles, gravity effect on horizontal struts, etc. As in other mechanical properties [5], the deviations in the geometry of the cells result in effective DD that may differ significatively form the nominal (pretended) DD obtained from a perfect geometry. Regarding the mathematical models, two different cases must be accordingly considered (Fig. 1): deviation of nodes located in the inner part of the cell (Fig. 1 bottom), and deviation

of the nodes located at the boundary of the cells (Fig. 1 top), the latter subjected to the Floquet-Bloch boundary conditions.

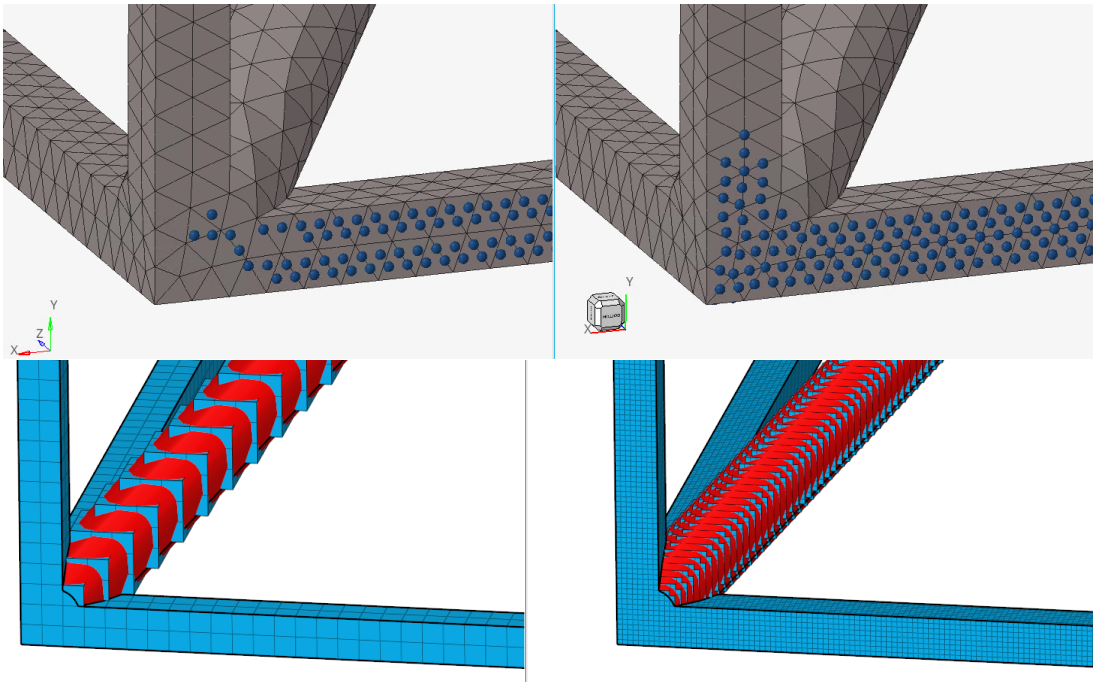

Figure 1: Distinction of nodal location cases. Top: nodes subjected to Floquet-Bloch Theorem boundary conditions. Bottom: internal nodes of the metamaterial cell.

2 Methodology. Cell definition

As an example, a specific cell has been designed in order to uncouple these two different cases, being cubic with 20mm size Fig. 2a. This cell has triple symmetry along the three coordinate planes which intersect in the geometric centre of the cell, belonging to $Pm\bar{3}m$ space group according to the international tables for crystallography [6]. Additionally, the boundaries of this cell are composed by solid parallelograms, while the inner part is composed of cylinder bars. This geometry has allowed to generate a fitted mesh and to separately control the numerical errors of both cases.

Even though this specific cell could be modelled with simpler methods, based on the cell symmetry and with the purpose of using generally applicable modelling methods, the fitted mesh has been produced through an automatic mesh with second order solid tetrahedral elements of one eighth ($1/8^{th}$) of the unitary cell geometry and thereby obtaining the whole cell applying the symmetries Fig. 2b. The cell geometry has been intentionally designed to be symmetric to facilitate this study, but it must be noted that not every lattice has geometrical symmetries and therefore the mesh-

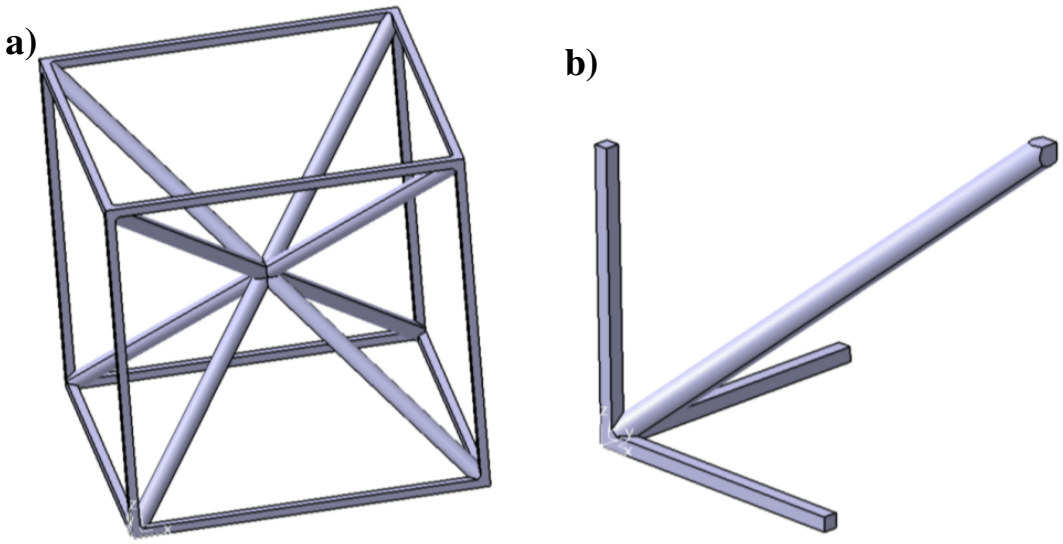

Figure 2: a) Cell Geometry: boundaries elements are parallelogram struts; inner elements are cylinders. b) $1/8^{th}$ Unitary cell for mesh fitting.

ing requirements for imposing the boundary conditions are not obtained directly with regular automatic meshing tools.

For imposing a maximum error at the boundaries, case 1, two different meshers readily available in any commercial finite element software to model any volume have been used for meshing the unit cell, in this case also with second order tetrahedral elements. Once the element size is selected and the geometry is meshed, the unfitted/not-fitted nodes subjected to periodic boundary conditions that exceed a maximum tolerance value with respect to the element size have been identified and replaced by nodes that perfectly match the nominal position Fig. 3. The geometry of the boundary is not modified from the nominal value, the deviation in the nodes subjected to periodic boundary conditions is studied in this work.

For imposing a maximum error within the cell, case 2, a different strategy, also typically available to modellers, has been followed. In this case, the mesh the unit cell is modelled with perfectly cubic hexahedral elements (which we shall refer to in this document as voxels; all having exactly the same size along the lattice). The study has been performed for first and second order elements. These elements can provide a perfect match of the geometry at the boundaries while the error of the inner geometry is related to the size of the voxel: the smaller the voxel is, better is geometry adjustment of the model (although for large voxel sizes, with the same dimension order of the characteristic length non-expected results may be obtained) Fig. 4. With this method, the approximate induced error is half the length of the major diagonal of the voxel.

The two cases analyzed in this work alter the hypothesis of infinite arrays of metamaterial cells: all the deviations in the position are considered as an infinite repeated deviation due to the imposed boundary conditions. Obviously, this differs from real

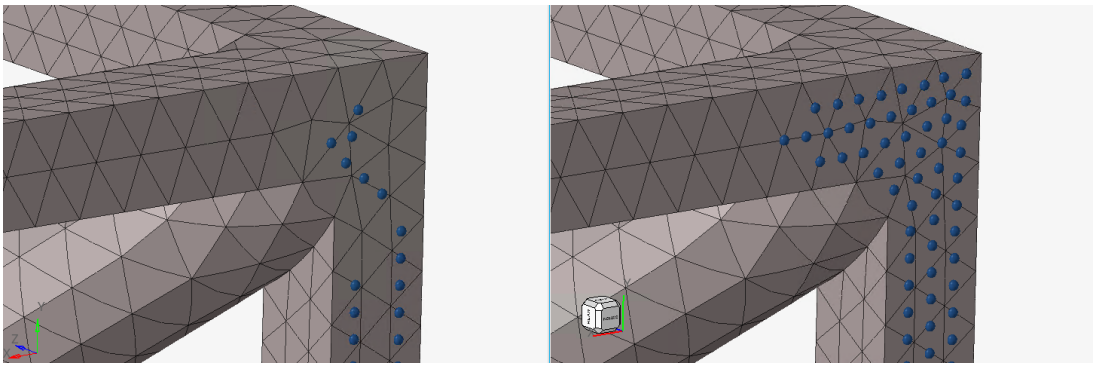

Figure 3: Numerical error at the boundaries. Nodes replaced highlighted; maximum allowed error wrt. element size 15% (left) and 1% (right).

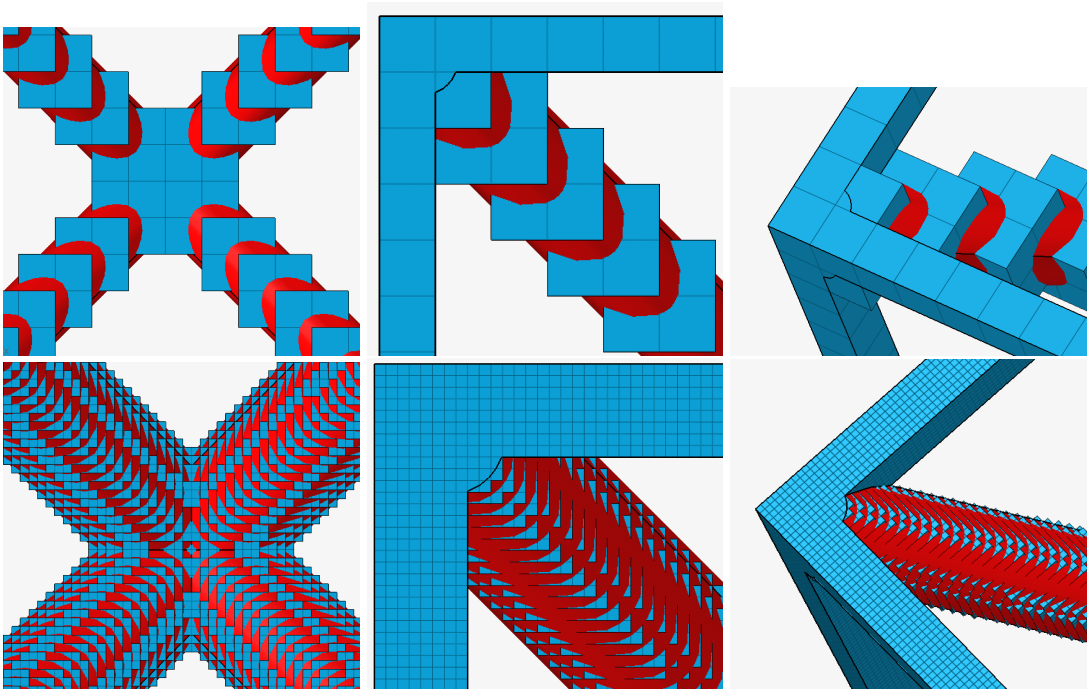

Figure 4: Meshes with voxel cubes, imposing error in position of nodes within the cell. Voxel characteristic sizes: 0.5mm (top) and 0.0625(bottom); imposed max. errors of 0.43mm and 0.05mm respectively.

structures, so that the purpose is to acquire a qualitative knowledge of the different sources of errors that must be considered when simulating the actual dynamic response of lattice-based MMM in a second step simulation. The accurate characterization of these geometric deviations in the response of the metastructure requires the simulation of the real finite geometry without periodic boundary conditions and with the selected unitary cell (which is usually selected in a previous trade-off of different single-cells among a collection of diverse options characterized through DD analysis) and their previously characterized deviations applied randomly along all the cells and finally applying the load cases.

3 Results

The studied cases are here presented:

3.1 Case 1: numerical errors at the boundaries

Tolerance % ES	0.04	0.1	1	5	10	15	20
Mesher A ES=0.25mm (FITTED)	✓					✓	
Mesher A ES=0.125mm (FITTED)	✓						
Mesher B ES=0.25mm (FITTED)					✓		
Mesher A ES=0.25mm (NOT FITTED)	✓	✓	✓	✓	✓	✓	✓
Mesher A ES=0.15mm (NOT FITTED)	✓		✓	✓	✓		

Table 1: Case 1. Numerical errors at the cell boundaries. Subcases performed (ES: element size)

Adimensional values have been selected in relation with the selected element size (ES). The element size has been selected according regular good practices in finite element modelling Fig. 5

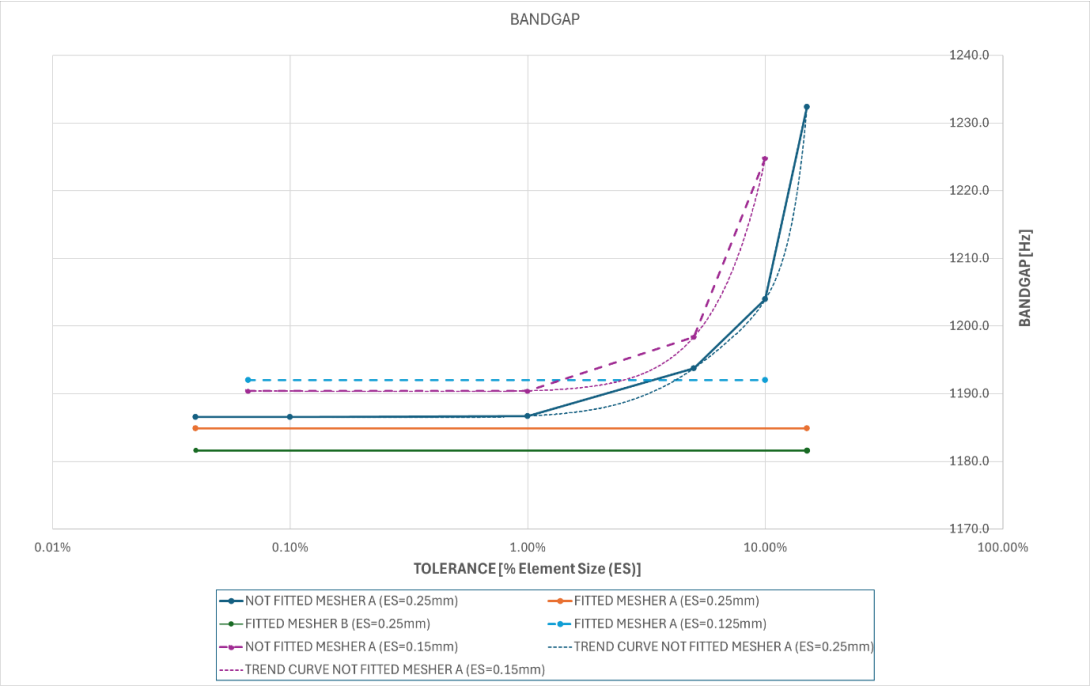

Figure 5: Case 1: Convergence trend of bandgap width depending on the used tolerance value. Mesh fitted results shown as horizontal lines for clarity (where necessary).

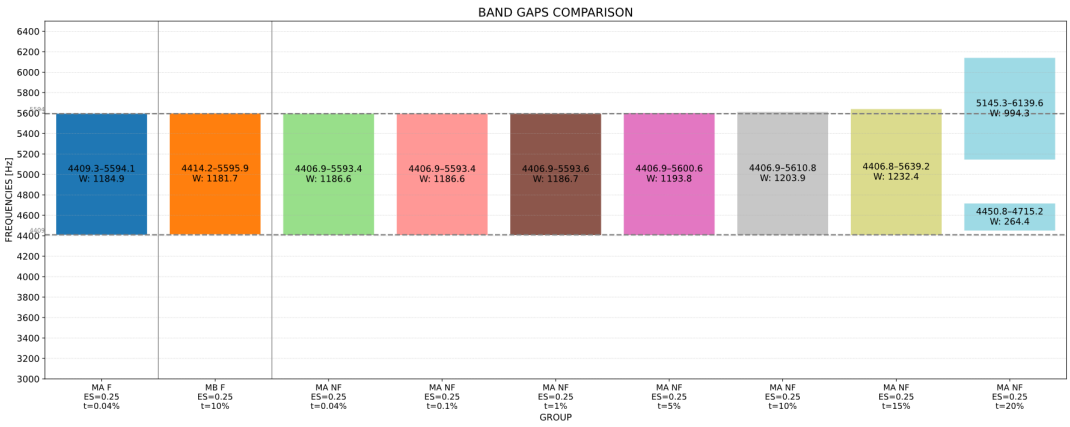

Figure 6: Case 1. Bandgaps obtained for the different subcases depending on the tolerance value used. MA: mesher A; MB: mesher B; F: fitted mesh; NF: not fitted mesh; ES: element Size [mm]; t: tolerance.

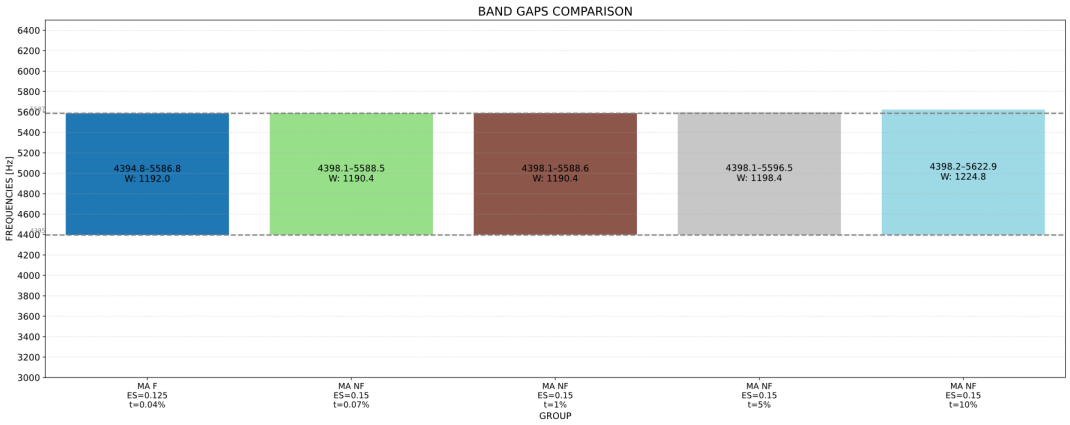

Figure 7: Case 1. Bandgaps obtained for the different subcases depending on the tolerance value used. MA: mesher A; F: fitted mesh; NF: not fitted mesh; ES: element size [mm]; t: tolerance.

3.2 Case 2: numerical errors within the cell.

#VOXELS PER SIDE	1^{st} **Order Hexa Elements**	2^{nd} **Order Hexa Elements**
39	✓	✓
40	✓	✓
80	✓	✓
120	✓	✓
160	✓	✓
200	✓	
320	✓	

Table 2: Case2. Numerical errors within the cell. Subcases performed

The analyses show that the convergence trend approximates to the target although the best result has still significant errors above the characteristic mathematical error of the method. A finer model would be required to match the target, but the selected minimum size of the voxels has been limited so that the number of degrees of freedom in the model do not exceed the value 10M DOF.

[H]

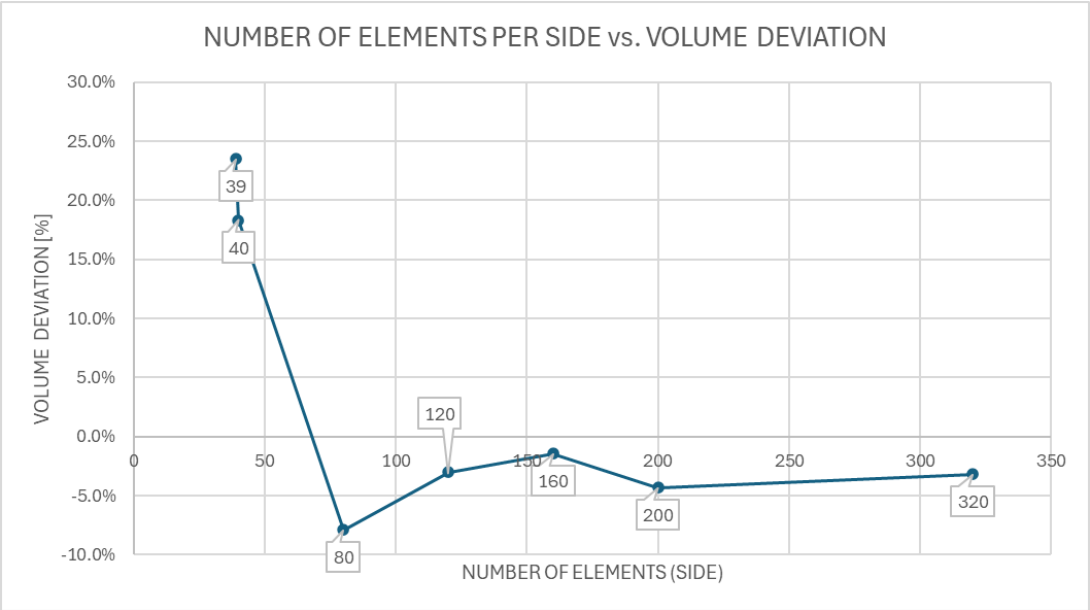

Figure 8: Case 2: Volume deviation of the subcases mathematical model wrt. target value (CAD geometry).

Fig. 8 demonstrates that decreasing the voxel size (equivalently, increasing the number of elements along each cell side) improves the agreement with the target volume, i.e. the geometric accuracy of the mathematical model. The algorithm used to replace the original geometry with voxels is such that when there is material at the nominal centre of a voxel, this voxel is activated. It can also be observed that this trend is oscillatory around the target volume, and in the subcase of 80 voxels the error becomes negative while for coarser meshes it was positive. This change of sign is highly significant on the DD shown bandgaps related with the influence of the mass and stiffness into the eigenmodes Fig. 9 and Fig. 10. For this specific geometry and specific studied bandgap, the excess of volume - with the associated change in mass and stiffness in the inner bars – suggests an increase in the mean value of the bandgap, thereby compensating the error in this study of the coarse subcases (39 and 40 voxels per cell side).

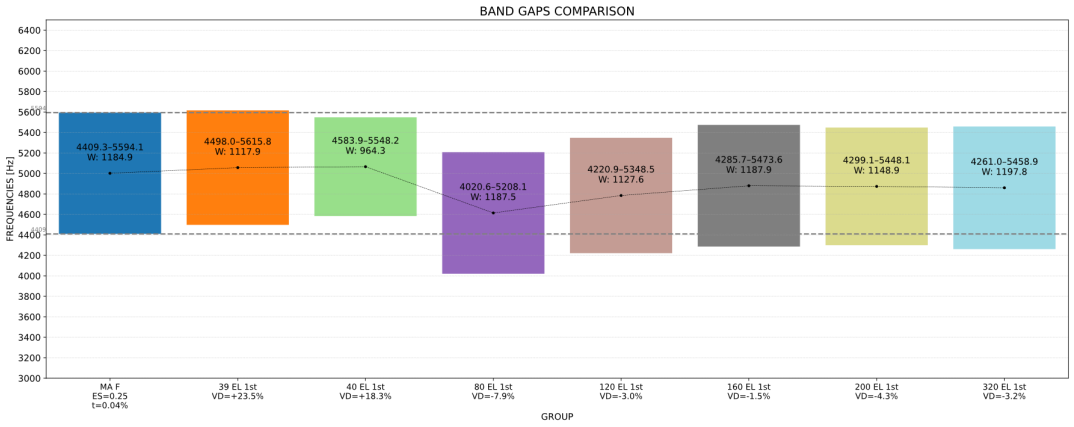

Figure 9: Case 2: 1^{st} Order hexa Elements. First column shows target (same code as Fig. 6); VD: volume deviation wrt. CAD geometry.

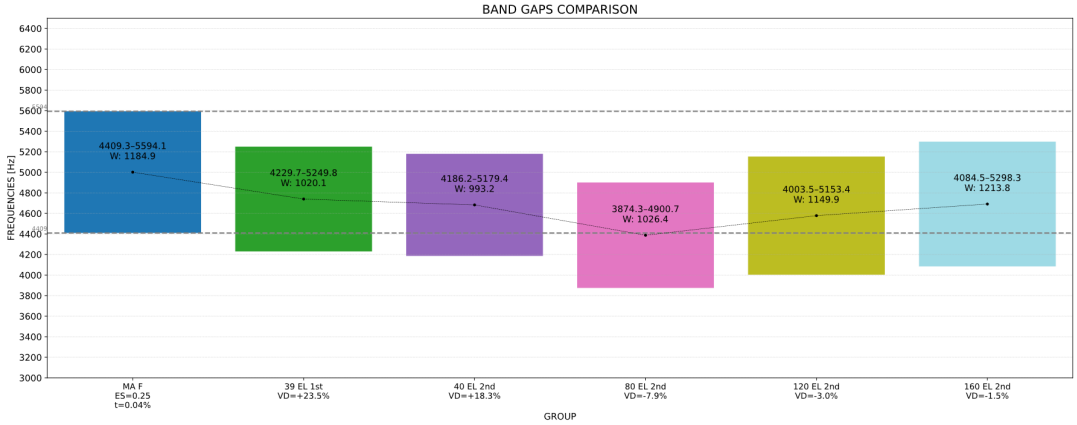

Figure 10: Case2: 2^{nd} Order hexa Elements. First column shows target (same code as Fig. 6); VD: volume deviation wrt. CAD geometry.

Results have been filtered in order to simplify their evaluation, removing small bandgaps below and above the studied bandgap, and verifying in all the subcases that the upper and lower branches which define the bandgap are associated at the same eigenmodes.

Expected outcomes can be observed from the results, the higher the number of voxels per lattice side, the better the agreement of the bandgap with the target value (the unexpected results for the coarse models have been commented on previously, related to the sign in volume deviation). Additionally, a second significant effect in the results is observed, where a lower mean value of the obtained bandgaps is produced due to second order elements. This effect is coherent with the lower stiffness of the second order elements.

4 Conclusions

This work highlights the different effect on the DD from two sources of numerical errors.

Case 1, numerical errors at the cell boundaries, where periodic boundary conditions apply. Here, the convergence to the level of the mathematical method is achieved when the maximum allowable error in position of boundary nodes is below 1% of the element size.

Case 2, numerical errors within the cell. The primary study results show that errors up to the 50% of the characteristic length of the struts used in a cell can deliver appropriate results for a primary study of a specific geometry provided that the deviation in volume of the cell is maintained below 20%. Further work is required to asses this conclusion and extend it to other lattice geometries.

Acknowledgements

This project has received funding from project BRISAS (PID2024-155747OA-C33), supported by MICIU/AEI/10.13039/501100011033, and by "ERDF A way of making Europe" and from the European Union's Horizon 2020 Marie Sklodowska-Curie Actions - Innovative European Training Networks under grant agreement No 956401.

References

[1] M. M. Sigalas, E. N. Economou, "Elastic and Acoustic Wave Band Structure", Journal of Sound and Vibration 158, no. 2, 377–82, 1992, DOI:10.1016/0022-460X(92)90059-7.

[2] P. Sheng, X. X. Zhang, Z. Liu, C. T. Chan, "Locally Resonant Sonic Materials", Physica B: Condensed Matter 338, nos 1–4, 201–5, 2003, DOI:10.1016/S0921-4526(03)00487-3.

[3] T. Meier, V. Korakis, B. W. Blankenship, et al, "Scalable Phononic Metamaterials: Tunable Bandgap Design and Multi-Scale Experimental Validation", Materials and Design 252, 113778, 2025, DOI:10.1016/j.matdes.2025.113778.

[4] W. Jiang, G. Yin, L. Xie, M. Yin, "Multifunctional 3D Lattice Metamaterials for Vibration Mitigation and Energy Absorption", International Journal of Mechanical Sciences 233, 107678, 2022, DOI:10.1016/j.ijmecsci.2022.107678.

[5] G. Vera-Rodríguez, L. Moreno-Corrales, I. Marín-González 1, Daniel Barba, F.J. Montáns, M.A. Sanz-Gómez, "Incorporation of Defects in Finite Elements to Model Effective Mechanical Properties of Metamaterial Cells

Printed by Selective Laser Melting", Sustainability 16(3), 1167, 2024, DOI:10.3390/su16031167.

[6] Th. Hahn (Editor), "International Tables for Crystallography, Vol. A: Space-Group Symmetry", Chichester, U.K., Wiley for the International Union of Crystallography, 2006, DOI: 10.1107/97809553602060000100.